Longitudinal Neutron Resonance Spin Echo Spectroscopy under Large Energy Transfers

C. Franz[1], O. Soltwedel[2], S. Säubert[1,2], A. Wendl[2], W. Gottwald[1], F. Haslbeck[2,3], L. Spitz[1] and C. Pfleiderer[2]

[1]Heinz Maier-Leibnitz Zentrum (MLZ), Technische Universität München, D-85748 Garching, Germany
[2]Physik Department, Technische Universität München, D-85747 Garching, Germany
[3]Institute for Advanced Studies, Technische Universität München, D-85747 Garching, Germanyny

E-mail: christian.franz@frm2.tum.de

Abstract. Longitudinal neutron resonance spin echo (LNRSE) spectroscopy offers very high energy resolution due to the self correction of the resonant spin flippers, and a wide dynamical range nominally exceeding six orders of magnitude in resolution down to sub-ps range. In this paper, the technical realisation how to achieve such low Fourier times at the spectrometer RESEDA at the MLZ Garching is described. The requirements of data collection and data analysis in the limit of very low Fourier times, notably those related to the breakdown of the spin echo approximation, are discussed. A method to infer the scattering function from the experimental data under large energy tansfers beyond the spin echo approximation is presented.

1. Introduction

Conventional neutron spin echo (NSE) spectroscopy [1] was developed to achieve ultra-high energy resolution, *i.e.*, to resolve extremely small energy transfers of the neutrons. Typically these high resolutions are required for studies of slow dynamical processes, as encountered, for instance, in protein dynamics [2], polymer physics [3], or the spin fluctuations in paramagnetic materials [4, 5]. Presently, the most advanced spin echo spectrometers offer resolutions of up to 1 μs [6, 7], corresponding to energy transfers of less than 1 neV at neutron energies of a few meV.

To fully benefit from the high energy resolution a large dynamic range proves to be essential. Lowest Fourier times in NSE are limited by the use of the shortest possible wavelength and minimal magnetic precession field only around the sample region with additional $\pi/2$ flippers (sometimes referred as "shorty" option). The magnetic field is just enough to retain the neutron beam polarisation over the whole instrument [8]. In combination, in conventional NSE spectrometers the shortest Fourier times accessible are in the range of 3-4 ps, corresponding to energies of ~ 0.2 meV. This is realised by means of so-called shorties. However, shorties do not allow infinitesimally small field integrals as a minumum field must be retained to prevent depolarisation of the neutron beam. In turn, in conventional NSE spectrometers the shortest Fourier times accessible are in the range of 3-4 ps, corresponding to energies of ~ 0.2 meV. Moreover, the use of shorties at NSE instruments involves a reconfiguration of the entire set-up and may not be carried out directly. In general the maximum energy loss is given by the energy

of the incident neutrons, which is, for cold neutrons, in the range of $\sim$1-5 meV, the energy transfer on the energy gain side may be much larger as, for example, in time-of-flight methods.

Longitudinal neutron resonance spin echo (LNRSE) and longitudinal modulation of intensity with zero effort (LMIEZE) are able to overcome the limits of classical NSE for high energy transfers by means of an effective field subtraction method [9].Namely, a field integral generated with a conventional NSE solenoid is used to reduce the field integral generated by the resonant spin flippers. This way, in principle, infinitesimally small Fourier times may can be reached, while the beam polarisation is retained. In turn, LNRSE and LMIEZE are able to cover an exceptionally large dynamic range from meV to neV energy transfers, elegantly encompassing several different spectroscopic techniques, notably time-of-flight, backscattering, and classical spin echo. However, measuring energy transfers in the meV range using spin echo is not straightforward as complications concerning technical realisation and data treatment arise. In this paper we report the technical realisation of ultra-short spin-echo times and a concomitant huge dynamic range at the beam-line RESEDA at MLZ in Garching [10], and the associated requirements of data reduction for LNRSE and LMIEZE.

2. Neutron Resonance Spin Echo Spectroscopy (NRSE)

In NSE spectroscopy energy transfers of the neutrons are encoded in the polarization as opposed to changes of wavelength. This way the energy resolution of the instrument is decoupled from the wavelength spread. The encoding is realized by virtue of the Larmor precession in an optimized magnetic field generated with carefully designed large solenoids. In comparison, in NRSE an equivalent Larmor labelling is implemented by means of a set of two radiofrequency(rf) spin flippers separated by a distance L that corresponds to the length of the NSE solenoid. The rf-flippers comprise two coils, one generating a strong static magnetic field B_0 and an oscillatory magnetic field B_1. The strong static magnetic field may be oriented perpendicular to the neutron beam, referred to as transverse NRSE (TNRSE) or in neutron flight direction, referred to as longitudinal NRSE (LNRSE). In comparison, the oscillatory field is always perpendicular to both the neutron beam and the static magnetic field direction. Field values are chosen as to achieve the resonance condition

$$\omega = \gamma B_0, \tag{1}$$

with γ being the gyromagnetic ratio and B_0 the static magnetic field. In a classical account, the phase angle Φ_{NRSE} of the neutron after the second rf-flipper is equal to the phase collected when travelling through the primary spectrometer arm

$$\Delta\Phi_{\mathrm{NRSE}} = 2\frac{\gamma B_0 L}{v} - \frac{\gamma B_{\mathrm{nse}} L_{\mathrm{nse}}}{v}, \tag{2}$$

with the static magnetic field B_0, the zero field region between the rf-flippers L, the field of the subtraction coil B_{nse}, the length of the subtraction coil L_{nse}, and the neutron velocity v. The first term in Eq. (2) corresponds to the phase collected in a conventional NSE solenoid with a factor of two arising from the resonant flip. The second term in Eq. (2) is the phase generated by the subtraction coil between the rf-flippers. As indicated by the minus sign, even though the precession field is pointing along the neutron flight direction, contributions to the field integral may be subtracted while avoiding zero field areas where the neutron beam would depolarise.

A semiclassical depiction of a LNRSE instrument is shown in Fig. 1. The spin manipulating devices are shown in Fig. 1 (a). The potential energy of the neutron spin eigenstates 'up' and 'down', shown in Fig. 1 (b), is the Zeeman energy of the spin in the magnetic field. The evolution of the energies are 'exchanged' at the resonant flip. As magnetic fields are conservative, the kinetic energy, shown in Fig. 1 (c), has to balance the potential energy gain or loss of the eigenstates. These different kinetic energies lead to a flight time difference of the eigenstates

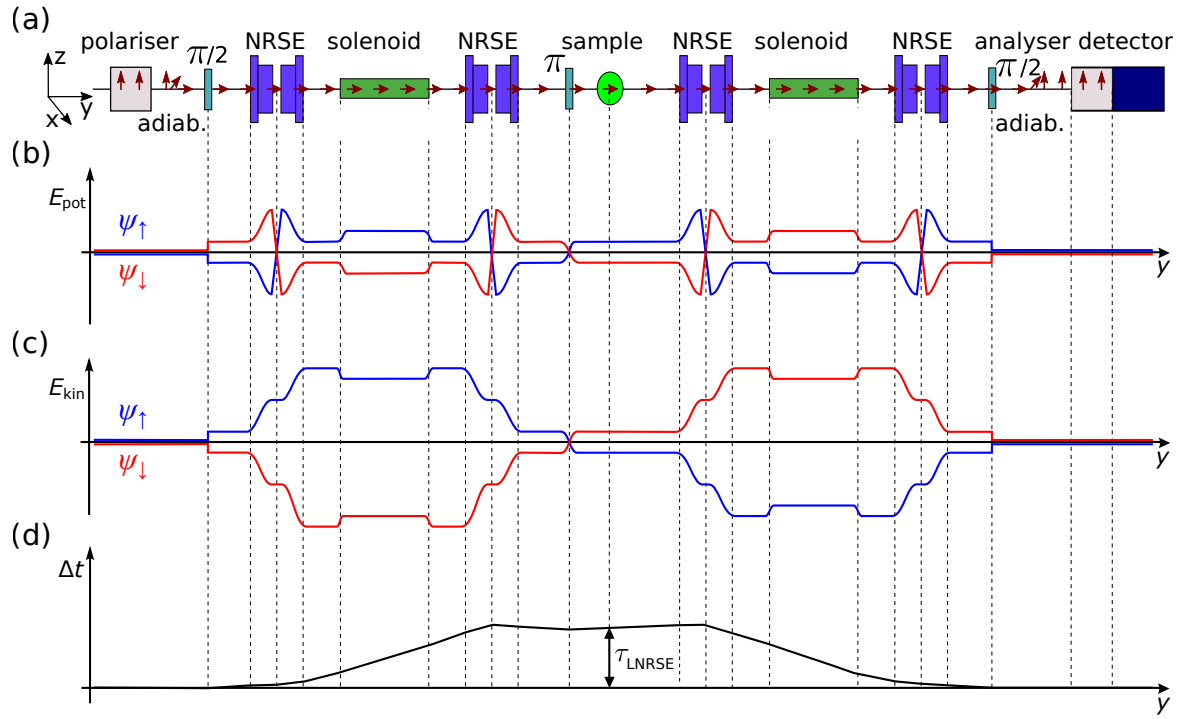

Figure 1. Qualitative depiction of longitudinal neutron resonance spin echo (NRSE) spectroscopy. (a) Schematic set-up of a longitudinal neutron resonance spin echo spectrometer. (b) Potential energy of the neutron wave function for spin up and down states, respectively. (c) Corresponding kinetic energy of the spin states. (d) The temporal splitting of the two spin states.

shown in Fig. 1 (d). The temporal splitting at the sample position corresponds to the spin echo time τ_{NRSE}. A field generated by the additional solenoids between the rf-flippers on both spectrometer arms may be used to subtract field integral, leading to a reduction of the splitting at the sample position.

A minimum frequency, and corresponding static field, for the resonant spin-flip is given by the Bloch-Siegert shift [11, 12]. The rotating magnetic field is realised by the decomposition of one linear oscillatory field into two counter-rotating fields. One component matches the Larmor precession of the neutron, the other component is far from resonance. It may be treated as a small disturbance to the static field B_0 as long as the amplitude is significantly smaller, *i.e.* $B_1 \ll B_0$. For a wavelength of $\lambda = 6$ Å and a flipper length of $d = 1.8$ cm, a field of $B_1 = 6.3$ G is required for inducing a π-flip in the neutron spin. For $B_0 \geq 2 \cdot B_1$ a minimum frequency of 35 kHz is necessary, yielding a field integral of 4.7 mTm with coil distance $L_1 = 1.87$ m at RESEDA.

As mentioned above, to reduce the field integral generated by the rf-flippers, a solenoid is placed between them. The requirements are here that the solenoids must provide sufficient field integral, have good homogeneity over the beam diameter, and create only little stray fields at the location of the rf-flipper. Following Zeyen and Rem [13] an optimal field shape geometry was chosen for the set-up at RESEDA. The length of the solenoid is $L_{nse} = 1$ m with a diameter of $d = 0.2$ m. It features five layers in a $\cos^2$ geometry, providing sufficient field integral of 5.73 mTm at a current of $I = 2.2$ A with a maximum inhomogeneity of 613 ppm for a beam with a diameter of 4 cm [14].

To obtain the spin echo time in N(R)SE we start with the neutron spin phase accumulated

in a field B_0 or between two resonant flippers with static field B_0 respectively

$$\Phi = (2)\gamma B_0 \cdot t = (2)\gamma B_0 \frac{L}{v}, \tag{3}$$

where t is the time spent in the field, L is the length of the field region, and v represents the velocity of the neutron. In the case of NRSE, an additional factor 2 is gained due to the resonant flip. The total phase accumulated before and after the sample in N(R)SE is given by

$$\Phi = \Phi_1 - \Phi_2 = \left((2)\gamma \frac{B_{0,1}L_1}{v_1} - \gamma \frac{B_{nse,1}L_{nse}}{v_1}\right) - \left((2)\gamma \frac{B_{0,2}L_2}{v_2} - \gamma \frac{B_{nse,2}L_{nse}}{v_2}\right) \tag{4}$$

$$= \gamma((2)B_0L - B_{nse}L_{nse})\left(\frac{1}{v_1} - \frac{1}{v_2}\right) \tag{5}$$

$$= \gamma((2)B_0L - B_{nse}L_{nse})\left(\frac{1}{v} - \frac{1}{v+\Delta v}\right), \tag{6}$$

where $B_{0,1} = B_{0,2} = B_0$, $B_{nse,1} = B_{nse,2} = B_{nse}$, $L_1 = L_2 = L$, $v_1 = v$, and $v_2 = v + \Delta v$. It should be noted that the minus sign is due to the π-flip between the two spectrometer arms. In case of small energy transfers, *i.e.*, $\Delta v \ll v$, a Taylor expansion gives

$$\Phi \approx \gamma((2)B_0L - B_{nse}L_{nse})\frac{\Delta v}{v^2}. \tag{7}$$

The change in velocity due to the scattering process in terms of energy transfer may be expressed as

$$\Delta E = \hbar\omega = \frac{m_\mathrm{n}}{2}\left((v+\Delta v)^2 - v^2\right) \tag{8}$$

$$= \frac{m_\mathrm{n}}{2}\left(2v\Delta v + \Delta v^2\right) \tag{9}$$

$$\approx m_\mathrm{n} v \Delta v. \tag{10}$$

Using the Planck constant $\hbar$ and the mass of the neutron m_n allows to rewrite Eq. (7) as

$$\Phi = \gamma((2)B_0L - B_{nse}L_{nse})\frac{\hbar}{m_\mathrm{n}v^3}\omega =: \tau_{\mathrm{N(R)SE}}\omega, \tag{11}$$

where the spin echo time is defined as

$$\tau_{\mathrm{N(R)SE}} = \frac{\gamma\hbar((2)B_0L - B_{nse}L_{nse})}{m_\mathrm{n}v^3}. \tag{12}$$

3. Modulation of Intensity with Zero Effort (MIEZE)

In contrast to NRSE, the so-called Modulation of Intensity with Zero Effort (MIEZE) represents a high resolution time of flight (TOF) method, using only the primary NRSE spectrometer arm. The MIEZE setup is schematically shown in Fig. 2 (a). In comparison to NRSE, the rf-flipper are now operated at different frequencies $\omega_{a,b}$. After the first flipper, the phase is the same as in NRSE

$$\Phi_a = 2\omega_a t_a. \tag{13}$$

We follow the derivation of Keller *et al.* [15], who provide a detailed introduction of the MIEZE technique. Since the second flipper is operated at a different frequency, the neutron spin phase

after the second flipper is modulated in time with a frequency given by the double difference of both flipper frequencies

$$\Phi_b \;=\; 2(\omega_b - \omega_a)t + \frac{2\omega_b L_1}{v} - \gamma\frac{B_{nse}L_{nse}}{v}. \tag{14}$$

Due to the individual velocities v for neutrons in a polychromatic beam, the amplitude modulation can only be seen at the echo point in space. This spin echo point is given by the MIEZE condition

$$\frac{\omega_b - \omega_a}{\omega_a} - \gamma\frac{B_{nse}L_{nse}}{2L_2\omega_a} \;=\; \frac{L_1}{L_2}, \tag{15}$$

to which the instrument is tuned. Here, ω_a and ω_b represent the angular frequencies of the first and second rf-flipper, respectively, L_1 is the distance between the rf-flippers, and L_2 the distance from the second rf-flipper to the detector, as depicted in Fig. 2 (a). With the MIEZE condition the phase of the neutrons at the detector position is velocity independent with

$$\Phi_\mathrm{D} \;=\; 2(\omega_b - \omega_a)t_\mathrm{D}, \tag{16}$$

where t_D is the time of arrival at the detector. A spin analyser converts the phase of the neutron into signal intensity, which is modulated in time

$$I(t_\mathrm{D}) \;=\; I_0/2(\cos(\Phi_\mathrm{D}(t_\mathrm{D})) + 1). \tag{17}$$

It is important to note that the analyser may be placed anywhere between the second rf-flipper and the detector, especially in front of the sample position, making the signal independent of depolarising conditions downstream the analyser.

Finite energy transfers $\hbar\omega$ by the sample will change the neutron velocity and thus the arrival time at the detector. The phase of the neutron is then changed by

$$\Delta\Phi(\hbar\omega) \;=\; 2(\omega_b - \omega_a)L_\mathrm{SD}\Big(\frac{1}{v} - \frac{1}{\sqrt{v^2 + 2\hbar\omega/m_\mathrm{n}}}\Big). \tag{18}$$

The probability for a scattering event with energy transfer $\hbar\omega$ is given by the scattering function $S(\hbar\omega)$. To obtain the signal at the detector, the intensity for a change of phase by 2π is integrated over all energy transfers

$$I(t) \;=\; I_0/2\int S(\hbar\omega)(\cos(\Phi_\mathrm{D}(t) + \Delta\Phi_\mathrm{D}) + 1)\,\mathrm{d}\hbar\omega. \tag{19}$$

In case of small energy transfers, as typically encountered in quasi-elastic scattering, where

$$\hbar\omega \;=\; \Delta E \ll E_n \quad\Rightarrow\quad \Delta v \ll v, \tag{20}$$

the detailed balance is negligible and the scattering function $S(\hbar\omega)$ is symmetric. For these assumptions, the signal intensity becomes explicitly time dependent and may be written as

$$I(t) \;=\; I_0/2\int S(\hbar\omega)(\cos(\Phi_\mathrm{D}(t))\cos(\Delta\Phi_\mathrm{D}) + 1)\,\mathrm{d}\hbar\omega. \tag{21}$$

The amplitude of the time dependence is directly proportional to the contrast

$$C \;=\; S(\tau) \;=\; \int S(\hbar\omega)\cos(\omega\tau)\,\mathrm{d}\hbar\omega. \tag{22}$$

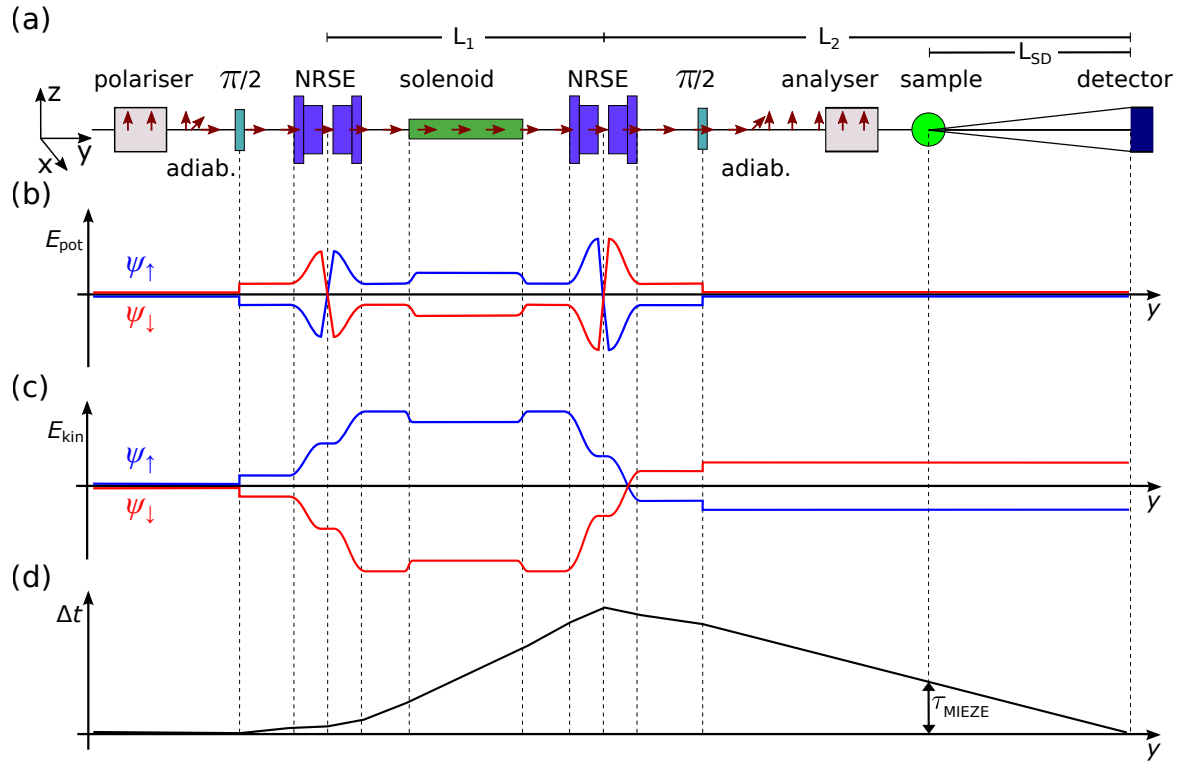

Figure 2. Qualitative depiction of Longitudinal Modulation of Intensity with Zero Effort (LMIEZE) spectroscopy. (a) Schematic set-up of a longitudinal MIEZE spectrometer. (b) Potential energy of the neutron wave function for spin up and down states. (c) Corresponding kinetic energy of the spin states. (d) Temporal splitting of the two spin states.

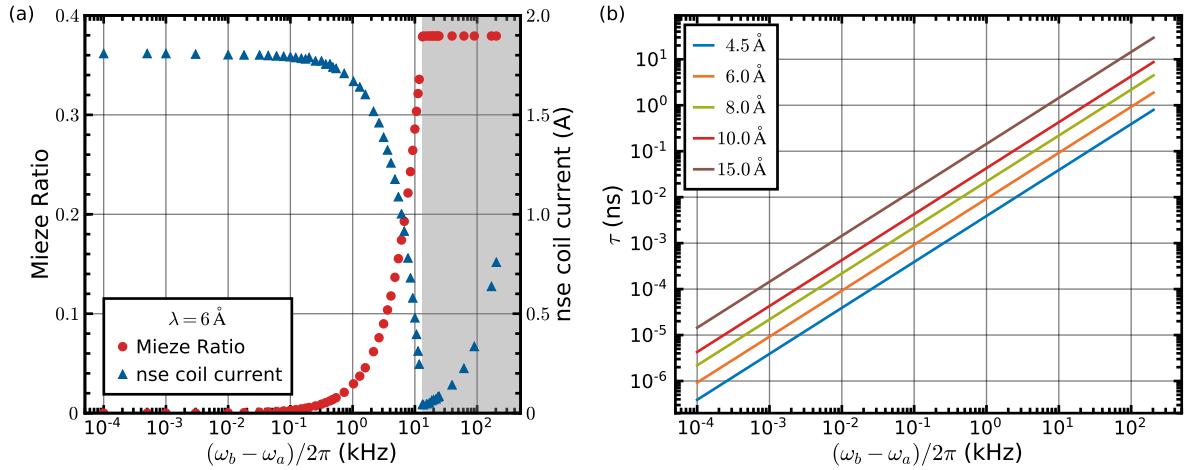

Figure 3. (a) MIEZE ratio and field subtraction coil (nse) current as a function of the frequency difference of the rf-flipper coils. The dark shaded area has a fixed MIEZE ratio of 0.375, the nse coil current increases as the detector is positioned a few mm short of the echo point. In the light shaded area the MIEZE ratio is small so that the MIEZE group has to be focused on the detector by an increased nse coil current. (b) Spin echo time as a function of MIEZE frequency on a double logarithmic scale for various wavelengths accessible at RESEDA. The resolution is linear in the frequency difference of the neutron intensity, but cubed in the neutron wavelength.

In addition, for small energy transfers the change of phase, $\Delta\Phi_{\mathrm{D}}$, is linear in energy as shown in Fig. 4 (a), namely

$$\Delta\Phi_{\mathrm{D}} \;=\; 2(\omega_b - \omega_a)\frac{\hbar L_{\mathrm{SD}}}{m_{\mathrm{n}} v^3}\omega \;=\; \tau\omega, \tag{23}$$

where the so-called MIEZE time, τ, has been introduced as a proportionality constant analogous to N(R)SE. Therefore, Eq. (22) takes the form of a cosine Fourier transform, and the contrast may be identified with the intermediate scattering function, *i.e.*, $C = S(\tau)$.

For the case of LMIEZE increasing the dynamic range involves further requirements that differ from those required in LNRSE. Namely, the ratio L_2/L_1 of the distance between the two rf-flippers, L_1, and the distance between the second rf-flipper to the detector, L_2, is fixed. As explained above this determines the frequency ratio ω_b/ω_a, according to the MIEZE condition. The implications for changes of the field integral are illustrated in Fig. 3 (a), which displays the MIEZE ratio (axis on the left hand side) as a function of the frequency difference $\Delta\omega = \omega_b - \omega_a$ and thus the Fourier time τ.

In the dark shaded area on the right hand side the MIEZE ratio is fixed at 0.375. The detector is placed just a few mm in front of the calculated spin echo point such that the focusing may be done by subtracting field integral with the NSE-type solenoid. Therefore, the current in the NSE-type solenoid increases with increasing frequency difference in the dark shaded area.

Without field integral subtraction the lowest accessible Fourier time is again given by the minimum frequency of the first rf-flipper, which is 35 kHz at RESEDA. To access smaller Fourier times, the MIEZE ratio has to be decreased, as indicated by the light shaded region of Fig. 3 (a), and the current in the NSE coil is increased to focus the echo point on the detector at distance L_2. This way, in principle, infinitesimally small Fourier times may be reached. Indeed, at RESEDA, a frequency difference of 0.1 Hz has been tested, resulting in an amplitude modulation of the neutron beam with a period of 5 s.

Taking into account the possibility of greatly reducing the field integral without loss of contrast Fig. 3 (b) shows the resulting Fourier times τ as a function of the frequency difference on a double logarithmic scale for various neutron wavelengths as available at RESEDA. The resolution is linear in the frequency difference, but cubed in the neutron wavelength. The specific choice of wavelength in any given experiment depends on the neutron flux, which has its maximum at 4 Å at RESEDA, as well as the desired q-range and resolution, and the reduction of contrast due to path-length differences in large samples as presented in Refs. [16, 17].

4. Limitations for Short Fourier Times

As discussed in the previous section, LMIEZE and LNRSE allow to reach much shorter Fourier times as compared to classical NSE. In the following, the complications arising from these short time-scales are addressed and the interpretation of the corresponding spin echo signal will be discussed. The phase of the neutron spin considered in Sec. 3 was derived under the assumption of the spin echo approximation, assuming a scattering process where the energy transfer between neutron and sample is much smaller than the energy of the incident neutron, *i.e.*, $\Delta v \ll v$. This may be satisfied for quasi-elastic scattering and inelastic scattering with low energy transfers. In case of larger energy transfers, the spin echo approximation fails.

To illustrate these effects, Fig. 4 (b) displays a typical scattering function as may be found in paramagnetic systems. A study of Ho2Ti2O7 [18] featuring the effects considered in the following will be presented elsewhere [19, 20]. A sharp quasi-elastic line represents the slow spin dynamics in the crystal field ground state. Additionally, transitions between crystal field levels can be observed at elevated temperatures. Such transitions have larger energies, in this example ~ 3 meV, exceeding the limits of the spin echo approximation. The temperature effects need to be considered in the scattering function according to detailed balance, making the scattering

function asymmetric. Therefore, the intensity at the detector is calculated via Eq. (19), taking into account a finite wavelength distribution $f(\lambda)$,

$$I(t) \;=\; \int f(\lambda)\mathrm{d}\lambda \int_{(-E_\mathrm{n},\infty)} S(\hbar\omega)(\cos(\Phi_\mathrm{D}(t)+\Delta\Phi_\mathrm{D})+1)\,\mathrm{d}\hbar\omega. \tag{24}$$

For computational reasons, the upper boundary is chosen to assume a finite value at which the scattering function is essentially zero. It is important to note that Eq. (24) no longer assumes the form of a cosine Fourier transform and the analytic expression may not be applied (Eq. (22)). However, the intensity is still modulated in time, providing a cosine signal

$$I(2(\omega_b-\omega_a)t) \;=\; A\cos(2(\omega_b-\omega_a)t+\phi)+M, \tag{25}$$

where the phase ϕ and the amplitude A are unknown, and the mean value of the signal $M = I_0/2$ and the frequency $2(\omega_b-\omega_a)$ are known. Hence, Eq. (25) has to be calculated at $2(\omega_b-\omega_a)t = 0$ and $\pi/2$ to extract the amplitude

$$A \;=\; \sqrt{I(0)^2+I(\pi/2)^2} \tag{26}$$

and phase ϕ. This allows to determine the contrast $C := A/M$.

Taking into account that the integral in Eq. (24) is zero for $E \leq -E_n$, normalisation of the scattering function, $\int_{(-\infty,\infty)} S(\hbar\omega)\,\mathrm{d}\hbar\omega = 1$, has to be carried out numerically. However, comparing the integrals $\int_{(-\infty,\infty)} S(\hbar\omega)\,\mathrm{d}\hbar\omega$ and $\int_{(-E_n,\infty)} S(\hbar\omega)\,\mathrm{d}\hbar\omega$, the numerical Fourier transform of $S(\omega)$ leads to the correct limit of $S(Q,\tau\rightarrow 0) = 1$ and the normalisation of the scattering function can be retained.

Illustrated in Fig. 4 (c) is the need for such corrections, where the intermediate scattering function to the model from Fig. 4 (b) is plotted for both the numerical approach described above and the calculation using the direct Fourier transform with the spin echo approximation in the same model. The narrow quasi-elastic line with $\Gamma = 6.5\mu$eV corresponds to the exponential decay in the intermediate scattering function above 0.1 ps, which coincides for both approaches. Differences can be seen at the oscillation in the intermediate scattering function, corresponding to the 3 meV excitation, which shows a lower frequency when using the corrections. Hence, if the blue curve would be fitted by means of the spin echo approximation, the excitation energy would appear to be too low. Taken together, it can be seen that the effect of the correction becomes more pronounced, when the energies increase. We note that in this example a q-independent excitation is assumed, making the analysis straight forward. However, in general the coupling between energy transfer, scattering angle and momentum transfer has to be taken into account as for all direct geometry spectrometers.

5. Conclusions

We report the technical realisation of infinitesimally small Fourier times and a huge dynamic range by virtue of an effective field integral subtraction method at the longitudinal resonance spin echo spectrometer RESEDA (MLZ). We show that limitations due to beam depolarisation arising in conventional NSE at very low field integrals may be overcome in LNRSE by means of subtraction of field integral through a conventional NSE coil. As the static field components at all points is oriented along the path of the neutrons, no depolarisation of the beam may occur even in the limit of zero field integral. However, the breakdown of the spin echo approximation at energy transfers of the order of the neutron energy makes a numerical analysis of the scattering function $S(Q,\omega)$ mandatory. Nevertheless, using appropriate models, contrast and phase information may be extracted. With this, LNRSE allows to explore a wide range of neutron energy transfers starting from few neV up to to several meV in the same experiment. This requires normally the

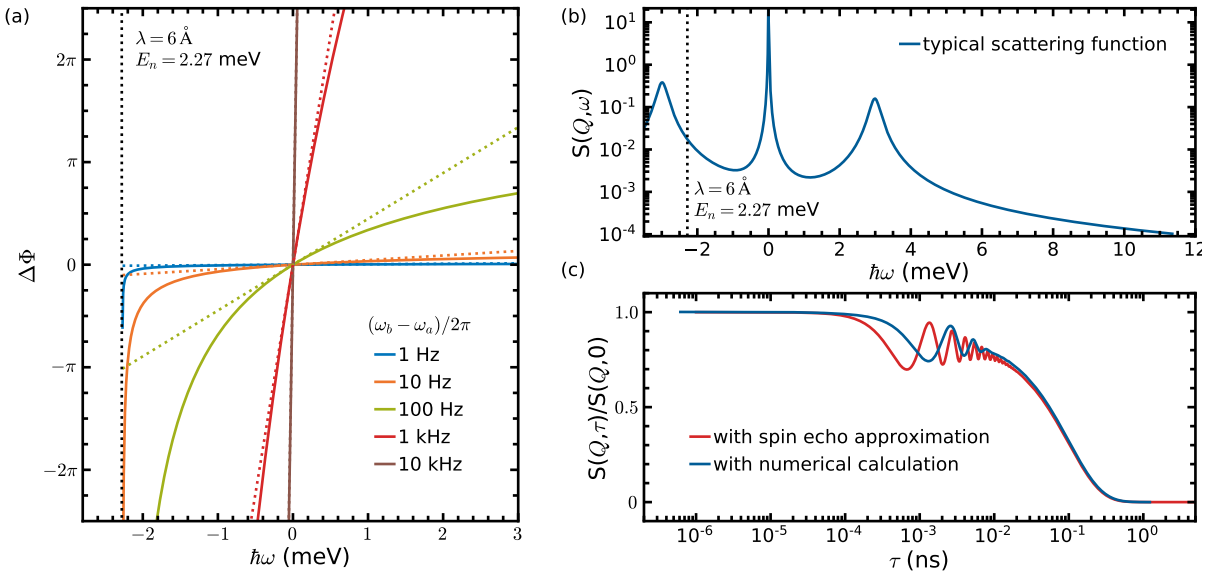

Figure 4. (a) Spin echo phase as a function of energy transfer for different MIEZE frequencies calculated with (dashed) and without (solid) the spin echo approximation. (b) Typical inelastic signal consisting of one quasi-elastic line with $\Gamma = 6.5\,\mu$eV and an inelastic transition with $E = 3$ meV, where the two peaks are weighted according to detailed balance. The dashed line represents the cut-off energy defined by the incident neutrons. (c) Comparison between spin echo approximation (red) and calculations using the explicit MIEZE phase (blue). Both curves use the scattering function from (b) as input.

combination of several spectrometers, namely conventional neutron spin echo, backscattering, time-of-flight, and triple-axis spectrometry. While this represents an important advantage of the the LNRSE/LMIEZE technique in its own right, the possibility to measure the intermediate scattering function directly is not possible by any other technique for an equivalent dynamic range.

Acknowledgements

We thank J. Kindervater, G. Ehlers, T. Keller, and C. Fuchs for advice and support. Financial support through the BMBF project "Longitudinale Resonante Neutronen Spin-Echo Spektroskopie mit Extremer Energie-Auflösung" (Förderkennzeichen 05K16WO6), DFG TRR80 (project F2), and ERC AdG 788031 (ExQuiSid) is gratefully acknowledged. F. Haslbeck was supported through a Hans Fischer fellowship of the Technische Universität München Institute for Advanced Study, funded by the German Excellence Initiative and the European Union Seventh Framework Programme under grant agreement no 291763. We also acknowledge support from the European Union through the Marie-Curie COFUND program.

References

[1] F. Mezei, Neutron spin echo: A new concept in polarized thermal neutron techniques, Zeitschrift für Physik A Hadrons and nuclei 255 (2) (1972) 146–160.
[2] D. J. E. Callaway, B. Farago, Z. Bu, Nanoscale protein dynamics: A new frontier for neutron spin echo spectroscopy, The European Physical Journal E 36 (7) (2013) 76.
[3] B. Ewen, Neutron spin echo investigations of polymer dynamics, Current Opinion in Solid State and Materials Science 3 (6) (1998) 606 – 609.

[4] G. Ehlers, A. L. Cornelius, T. Fennell, M. Koza, S. T. Bramwell, J. S. Gardner, Evidence for two distinct spin relaxation mechanisms in 'hot' spin ice $Ho_2Ti_2O_7$, Journal of Physics: Condensed Matter 16 (11) (2004) S635.
[5] F. Haslbeck, S. Säubert, M. Seifert, C. Franz, M. Schulz, A. Heinemann, T. Keller, P. Das, J. D. Thompson, E. D. Bauer, C. Pfleiderer, M. Janoschek, Ultrahigh-resolution neutron spectroscopy of low-energy spin dynamics in UGe_2, Phys. Rev. B 99 (2019) 014429.
[6] O. Holderer, O. Ivanova, J-nse: Neutron spin echo spectrometer, Journal of large-scale research facilities A11 (1).
[7] B. Farago, P. Falus, I. Hoffmann, M. Gradzielski, F. Thomas, C. Gomez, The IN15 upgrade, Neutron News 26 (3) (2015) 15.
[8] S. Pasini, O. Holderer, T. Kozielewski, D. Richter, M. Monkenbusch, J-nse-phoenix, a neutron spin-echo spectrometer with optimized superconducting precession coils at the mlz in garching, Review of Scientific Instruments 90 (4) (2019) 043107. doi:10.1063/1.5084303.
[9] M. Krautloher, J. Kindervater, T. Keller, W. Häussler, Neutron resonance spin echo with longitudinal dc fields, Review of Scientific Instruments 87 (12) (2016) 125110.
[10] T. S. C. Franz, Reseda: Resonance spin echo spectrometer, Journal of large-scale research facilities 1 (14). doi:http://dx.doi.org/10.17815/jlsrf-1-37.
[11] F. Bloch, A. Siegert, Magnetic resonance for nonrotating fields, Phys. Rev. 57 (1940) 522–527.
[12] U. Schmidt, Experimente mit polarisierten Neutronen zu Fragen der höchstaufgelösten Spektrometrie und Quantenoptik, Ph.D. thesis, Fakultät für Physik der Technischen Universität München Institut E21 (1995).
[13] C. M. E. Zeyen, P. C. Rem, Optimal larmor precession magnetic field shapes: application to neutron spin echo three-axis spectrometry, Measurement Science and Technology 7 (5) (1996) 782.
[14] W. Gottwald, Optimization and assembly of enhanced field integral substraction coils for the resonant spin-echo spectrometer RESEDA at MLZ, Bachelor's Thesis (2017).
[15] T. Keller, R. Golub, R. Gähler, Chapter 2.8.6 - Neutron spin echo - a technique for high-resolution neutron scattering, in: R. Pike, P. Sabatier (Eds.), Scattering, Academic Press, 2002, p. 1264.
[16] G. Brandl, R. Georgii, W. Häussler, S. Mühlbauer, P. Böni, Large scales-long times: Adding high energy resolution to SANS, Nuclear Instruments and Methods in Physics Research Section A: Accelerators, Spectrometers, Detectors and Associated Equipment 654 (1) (2011) 394 – 398.
[17] N. Martin, On the resolution of a MIEZE spectrometer, Nuclear Instruments and Methods in Physics Research Section A: Accelerators, Spectrometers, Detectors and Associated Equipment 882 (2018) 11 – 16.
[18] M. Ruminy, S. Chi, S. Calder, T. Fennell, Phonon-mediated spin-flipping mechanism in the spin ices $Dy_2Ti_2O_7$ and $Ho_2Ti_2O_7$, Physical Review B 95 (6).
[19] A. Wendl, Neutron spin echo spectroscopy on geometrically frustrated magnets, Master thesis, Technical University of Munich (2018).
[20] A. Wendl, S. Säubert, C. Duvinage, J. Kindervater, P. Dharmalingam, A. Boothroyd, C. Franz, C. Pfleiderer; MIEZE spectroscopy of dynamics and crystal field excitations in the classical spin ice system $Ho_2Ti_2O_7$ (2018).